Fracture Behavior Characterization of Amorphous Hydrogenated Silicon Carbide via Thin-Film Fracture Techniques

By Lorenzo Mangubat

Two samples of amorphous hydrogenated silicon carbide (a-SiC:H) were subjected to micro-tensile testing in the di-cantilever beam configuration to investigate their fracture behavior. One sample was found to have a strain energy release rate G_c almost eight times larger than the other. The difference was suspected to be a result of energy absorption by plastic absorption. Material plasticity was found to be higher in the sample that yielded a higher G_c. Results here combined with characterization data from previous work showed that this phenomenon is most probably due to the presence of polymeric regions in the a-SiC:H structure. The improvement in fracture resistance due to this phenomenon may improve the success of a-SiC:H as an engineering material.

Introduction

Amorphous hydrogenated silicon carbide (designated a-SiC:H) is a material of interest due to its chemical and thermal stability and tunable properties. Specifically, its structure can be adjusting by controling its chemical composition and processing conditions to perform optimally in applications ranging from microelectronic mechanical systems[2] to solar cells[4]. However, they are limited by their susceptibility to fracture due to the presence of terminal groups (i.e. C–H_x or Si–H_x) that decrease the material's network connectivity. The success of this material for engineering application thus relies on a thorough understanding and optimization of its fracture resistance.

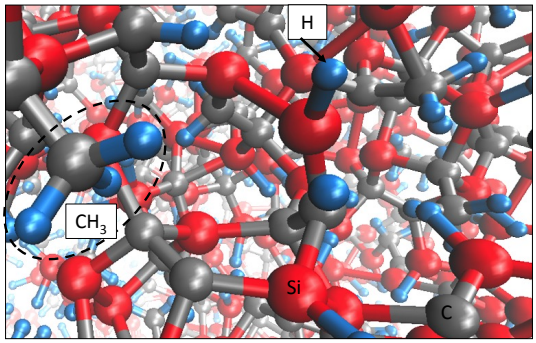

Figure 1: Structure of a-SiC:H. Silicon atoms are red, carbon atoms are grey and hydrogen atoms are blue. A terminal methyl group is encircled on the left. Other alkyl groups may be present but are not shown.

The key parameter for fracture resistance is the critical strain energy release rate G_c, which in general is expressed as:

$$G_c = \frac{P_c^2}{2B}\frac{dC}{da}\Big|_{a_c} \qquad \textbf{eq 1}$$

Where P_c is the applied load at crack growth, B is the sample thickness, h is the substrate height, C is the compliance, and a_c is the critical crack size. Using beam theory[1], G_c for a DCB sample can be written as:

$$G_c = \frac{12(1-\nu^2){P_c}^2}{EB^2h^3}\left(1 + 0.64\,\frac{h}{a}\right)^2 \qquad \textbf{eq 2}$$

Where ν is the substrate Poisson's ratio and E is the substrate Young's modulus. The size of the crack a for a DCB sample can be found using:

$$a = \left(\frac{CEBh^3}{8(1-\nu^2)}\right)^{1/3} - 0.64h \qquad \textbf{eq 3}$$

The micro-tensile apparatus can be used to evaluate G_c for a DCB sample. The apparatus consists of two grips that pull the two sections of the beam apart. The grips generate an electromagnetic signal which is proportional to the load. An actuator is able to measure the displacement.

In a typical tensile crack-propagation test, a material is loaded until a crack is formed as indicated by a sudden drop in load. The material can be periodically loaded and unloaded to generate linear regions to calculate compliance. A typical curve is shown:

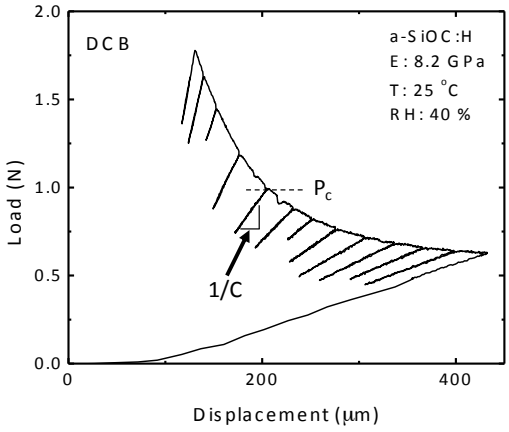

Figure 2: a typical load-displacement curve for a crack propagation experiment using micro-tensile testing. Image courtesy of Yusuke Matsuda of Stanford University.

The goal of this study was to evaluate the strain energy release rate G_c (and therefore the fracture resistance) of a-SiC:H via tensile micro-testing in the di-cantilever beam (DCB) configuration. The two samples evaluated were of very similar chemical composition yet showed significantly different G_c values. It is hypothesized that the higher G_c of sample 2 was due to energy absorbed by plastic deformation. This was the same phenomenon that lead Griffith to underestimate the observed critical strain energy release rate of materials[1]. Several experimental observations are described here to support this hypothesis. The analysis was augmented by results from nanoindentation, atomic force microscopy (AFM), X-ray photoelectron (XPS) spectroscopy, Fourier Tranform Infrared (FTIR) spectroscopy, and nuclear magnetic resonance (NMR Si and C^{13}) spectroscopy[1].

Procedure

Two a-Si:C:H samples were deposited on a 300mm silicon (0 0 1) wafer via plasma-enchanced chemical vapor deposition. Deposition time was calibrated to yield an a-Si:C:H layer 500 nm thick. Both top and bottom faces of this layer were passivated with 25nm thick layers of SiN to prevent diffusion of a-Si:C:H into the substrate. Passivation may also minimize oxidation. A top layer of silicon substrate was bonded with epoxy. The layering schematic is shown:

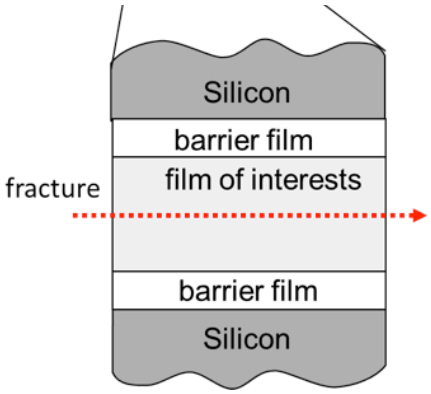

Figure 3: Layering of a-SiC:H samples used.

Both samples were designed to have similar chemical compositions. The nanoporosity diameter was 1 nm for both samples. Properties of both materials are summarized:

[1] Additional data provided by Yusuke Matsuda of Stanford University.

Table 1: Summary of properties for both samples.

Film designation	Density, ρ (g/cm^3)	Young's modulus, E (GPa)	Hardness, H (GPa)	Yield stress, σ_{ys} (MPa)	Porosity (vol.%)
a-SiC:H-1	1.1	6.4	0.85	792 ± 43	2
a-SiC:H-2	1.2	4.2	0.31	104 ± 11	12

Table 2: Compositions by atomic % of both samples.

	C	Si	O	H
a-SiC:H-1	30.2	10.6	9.6	49.6
a-SiC:H-2	38.6	5.0	4.3	52.2

Young's modulus was determined for both samples via nanoindentation hardness testing assuming a Poisson's ratio of 0.25. The yield stress was measured via the same method using the cavity model[3]. The indentation profiles are shown:

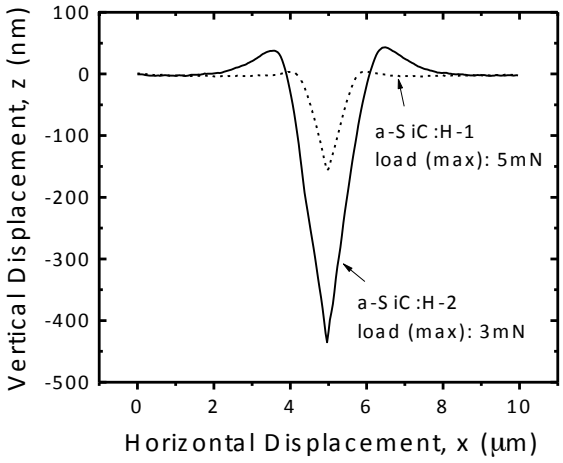

Figure 4: Surface profile generated via nanoindentation.

The following data were provided from previous work:

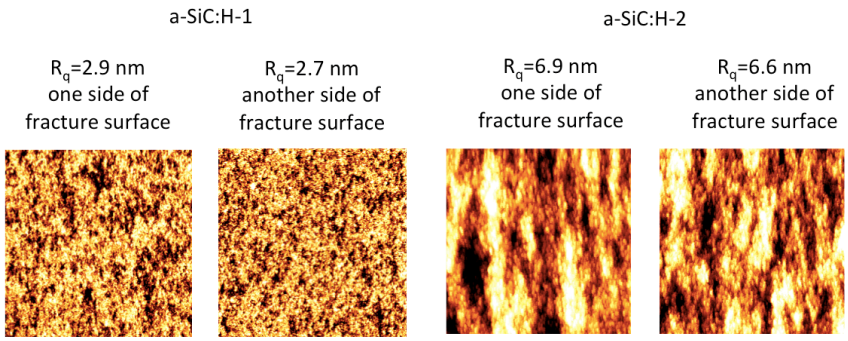

Figure 5: AFM topography for both samples with root-mean-squared roughness R_q.

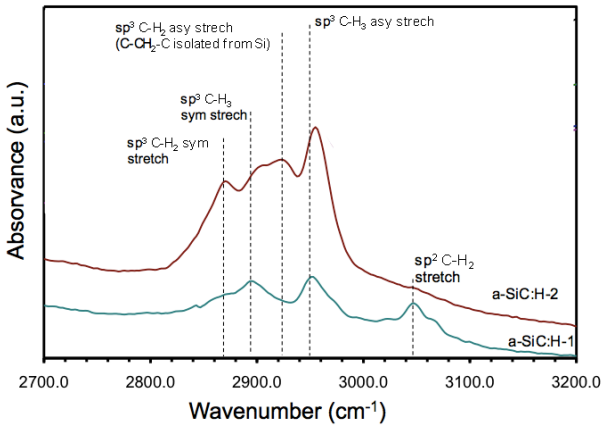

Figure 6: FTIR spectra for both samples.

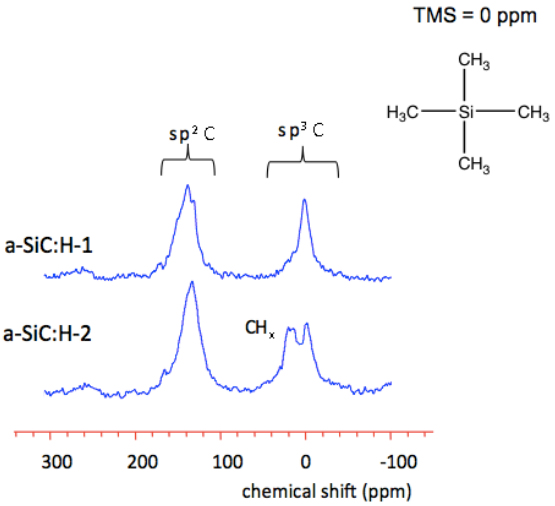

Figure 7: C^{13} NMR spectra for both samples referenced to TMS=0 ppm.

Both samples were subjected to micro-tensile testing until the calculated crack size was 28 mm. Each beam contained the following dimensions:

Table 3: Dimensions of samples.

	B [mm]	h [mm]	
a-SiC:H-1	4.54	0.780	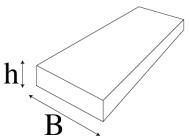
a-SiC:H-2	5.22	0.775	

The substrate Young's Modulus was 169 GPa and Poisson's ratio was 0.064. The samples were loaded and unloaded several times, and a G_C was calculated for each cycle. G_C was calculated based on the crack size at the onset of each cycle. Average values for G_C are reported, though only those with corresponding crack size greater than 20mm were averaged. If the crack size is too small, then G_C may not be in stead state.

After fracture, the surfaces of both materials were analyzed for chemical composition via XPS.

Results and Discussion

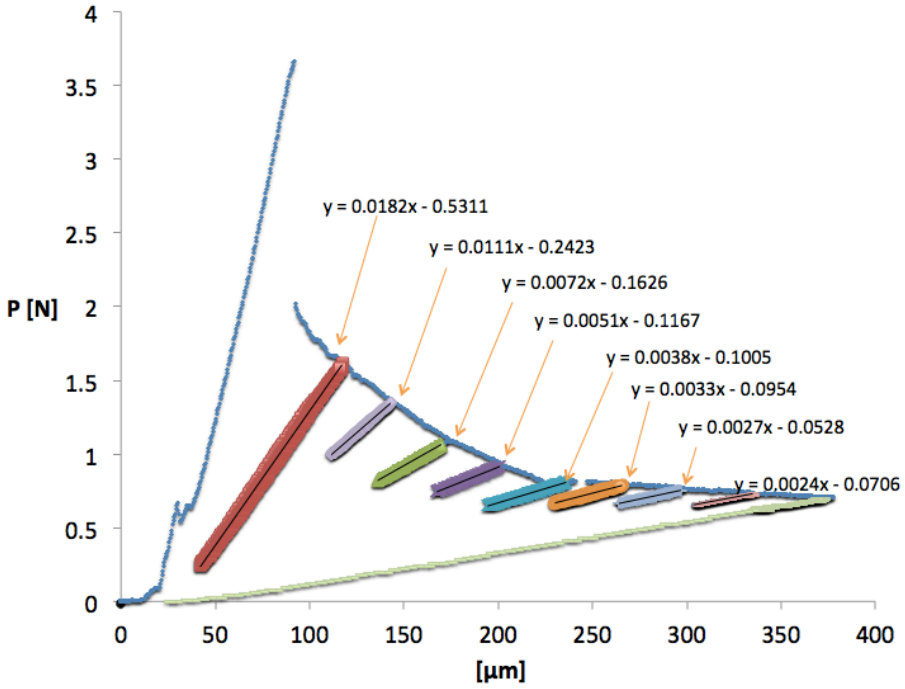

Figure 8: Load-displacement curve for sample 1. Linear fits per cycle for the calculation of compliance.

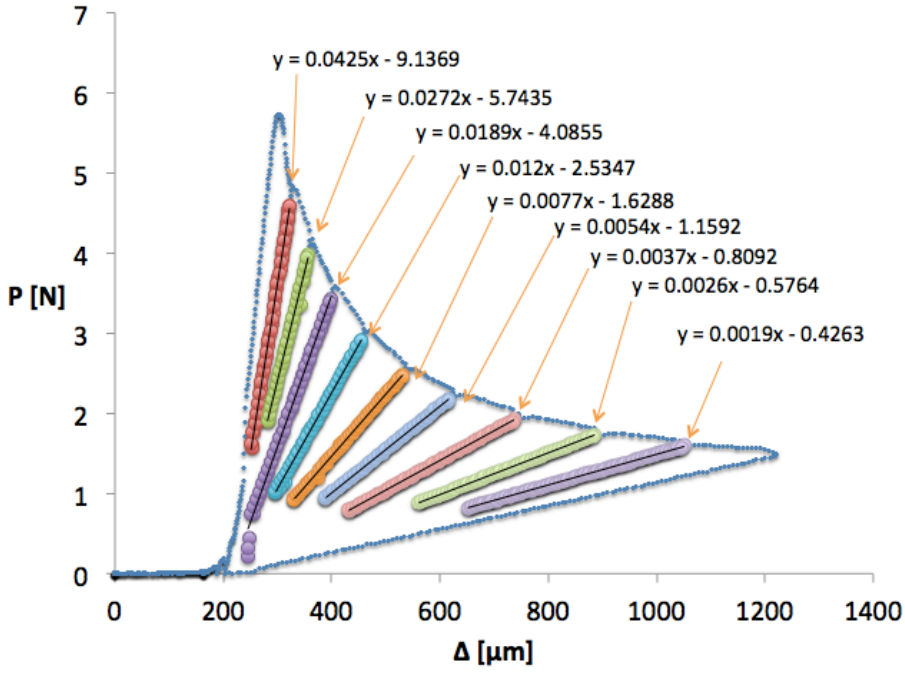

Figure 9: Load-displacement curve for sample 2. Linear fits per cycle for the calculation of compliance.

Table 4: Summary of critical strain energy release rate vs. crack size for both samples.

Sample 1		Sample 2	
a [mm]	**G_c [J/m^2]**	**a [mm]**	**G_c [J/m^2]**
20.27	2.63	20.72	11.94
22.41	2.48	23.57	11.98
23.52	2.59	26.57	12.28
25.18	2.72	29.55	12.82
26.20	2.77		
Average:	2.64	Average:	12.25
Std. dev:	0.11	Std. dev:	0.41

There is clearly a difference in the strain energy release rates for both samples (factor of 4.64). The difference cannot be attributed to chemical composition since they are very similar. Nor can it be attributed to crack path. Figure 10 and Figure 11 shows chemical structure that is symmetric between both sides for each sample. The binding energy for nitrogen (1s) is 410 eV and is absent in all spectra. Therefore the crack path never cut into the SiN passivation layers, and stayed on the a-SiC:H layer (cohesive fracture).

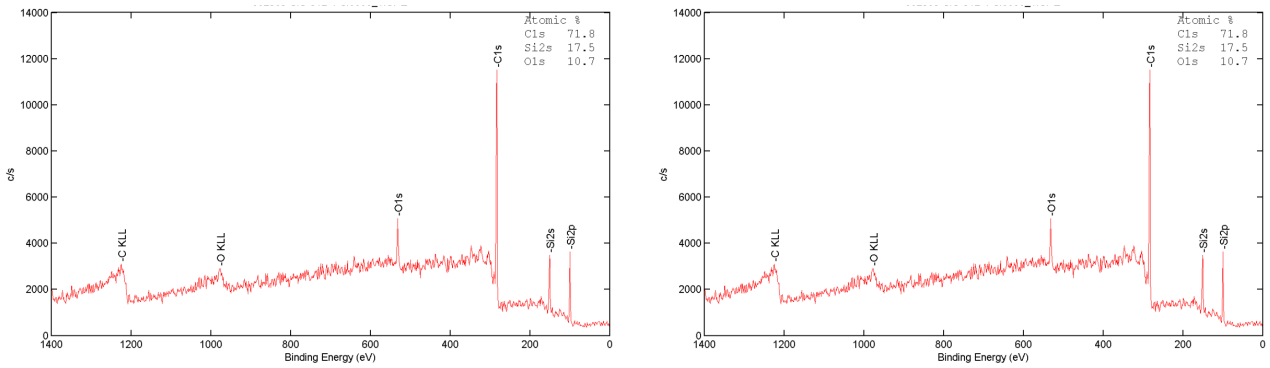

Figure 10: XPS spectra for sample 1 showing almost perfectly symmetrical composition.

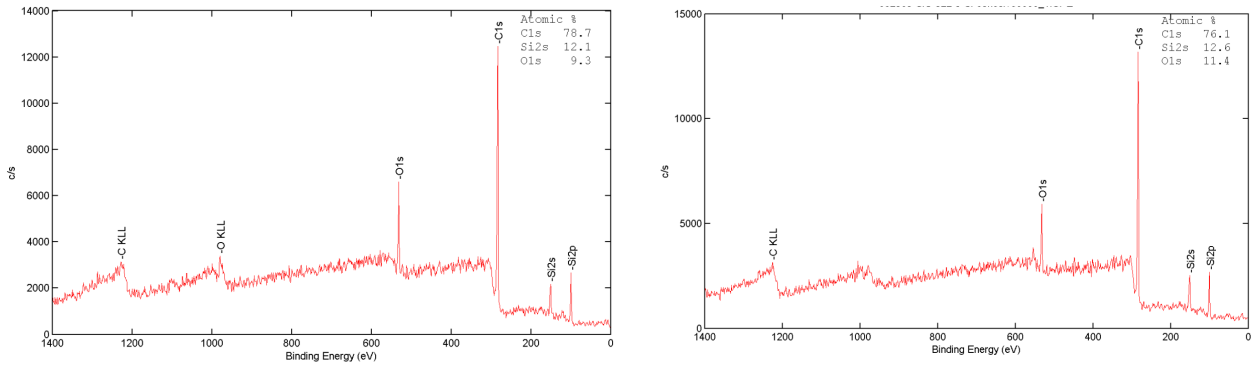

Figure 11: XPS spectra for sample 2 showing almost perfectly symmetrical composition.

The nanoidentation profile (Figure 4) is the first evidence of energy absorbance due to plasticity. The hardness of sample is lower based on the depth of indention for approximately the same amount of force. The measured yield strength for sample 2 is almost 8 times small than that of sample 1. Also note the pile-up of material around the indention surface area, which is another indication of plasticity.

The second indication of plasticity is the relative smoothness of the fracture surface as shown via AFM (Figure 5). Although it is not strong evidence, smoothness of the surface may be the result of plastic deformation dulling away any otherwise sharp features.

Polymeric regions could be responsible for the plasticity because polymers generally have low yield strength. There existence is evidenced in FTIR spectra (Figure 6). Sample 2 contains asymmetric $-CH_2$ stretching *away* from the silicon atoms. This can only occur when polymeric carbon chains are present.

Another evidence of the presence of polymeric regions is the C^{13}-NMR spectra. Sample 2 has one more peak than sample 1, indicating that it has a carbon environment not present in sample 1. Proposed environments for a carbon atom (red) are shown:

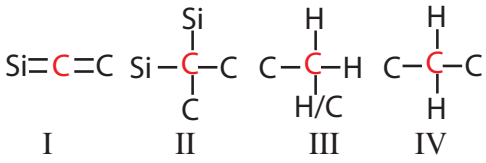

Figure 12: Different atomic units representing different environments for carbon.

Unit 1 is responsible for the peak at higher chemical shift and is present in both samples. Unit II is necessary for the material to have a solid structure and cannot be absent. Without unit IV, unit III can only exist adjacent to unit II and may be contribute to the same peak as unit II.Thus, only unit IV can exist uniquely in sample 2. This is the repeat unit for ethylene, which allows for polymeric regions in a-SiC:H.

It is highly probable that plasticity will result when significant polymeric regions are present. The strain energy can be converted to work done in changing the configuration or shape of polymers. A network of entangled polymers may be able to deform more easily without compromising bonds compared to a network of atoms with rigid bonds. Furthermore, polymers may cause bridging phenomenon that decrease the stress intensity at the rack tip as shown:

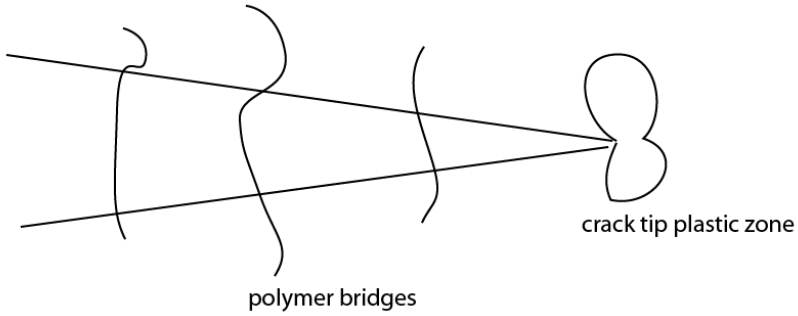

Figure 13: polymer bridging to reduce crack tip stress intensity.

The verify whether plasticity is indeed responsible for higher G_c values, the sample 2 film can be made thicker and re-tested. If the sample is too thin, then the plastic zone size is constricted by the a-SiC:H layer boundaries. If the film is made thicker, then the plastic zone can be larger and absorb more energy.

To further investigate the presence of polymers, the material can be subjected to typical polymer characterization techniques. The material can be subjected to shear stresses and observed for any dependence on time-related behaviors. For example, the shear modulus can be measured as a function of strain rate. Polymers are known to have at least notable dependence on shear strain rate. The material may also be tested at different temperatures within a small range such that the polymer configuration may be influenced without influencing the greater a-SiC:H structure. A slight increase in temperature may anneal the polymers and alter their mechanical properties.

Conclusion

Two samples of a-SiC:H were characterized for their strain energy release rate G_c and were found to have significantly different values. This difference was attributed to greater crack tip plasticity in sample 2, which may have been due to the presence of polymeric regions. This conclusion was supported with other characterization methods provided in previous work. Several observations were consistent with the presence of polymeric regions, and no observations suggested that they could not be present. The toughening of materials due to the presence of polymeric regions could prove instrumental in the

success of a-SiC:H as an engineering material. Existing polymer theories and techniques can be combined with fracture mechanics to further optimize this material.

Works Cited

1. Anderson, T.L. Fracure Mechanics: Fundamentals and Applications. Boca Raton: Taylor and Francis, 2005.

2. Avram, Marioara, et al. "Low stress PECVD amorphous silicon carbide for MEMS applications." Semiconductor Conference (CAS), 2010 International. 2010. 239 to 242.

3. W. Zielinski, H. Huang, and W. W. Gerberich. Journal of Materials Research 8.1300 (1993).

4. Ziegler, Johannes, et al. "Potentials and development of amorphous silicon carbide heterojunction solar cells." Fraunhofer Institute for Solar Energy Systems, Heidenhofstr. 2, 79110 Freiburg, Germany, n.d.